

# Strain localization phenomena associated with static and dynamic strain ageing in notched specimens: experiments and finite element simulations

S. Graff<sup>a,\*</sup>, S. Forest<sup>a</sup>, J.-L. Strudel<sup>a</sup>, C. Prioul<sup>b</sup>, P. Pilvin<sup>c</sup>, J.-L. Béchade<sup>d</sup>

<sup>a</sup> UMR 7633/Ecole des Mines de Paris/CNRS, Centre des Matériaux, BP 87, 91003 Evry, France

<sup>b</sup> MSSMAT, Ecole Centrale Paris, Grande Voie des Vignes, 92295 Châtenay-Malabry, France

<sup>c</sup> IUP Lorient, Université de Bretagne Sud, 2, rue Le Coat St-Haouen, 56325 Lorient, France

<sup>d</sup> SRMA, CEA Saclay, 91191 Gif sur Yvette, France

Received 26 August 2003; received in revised form 17 February 2004

## Abstract

The aim of the present work is to use an available constitutive model for the description of the Portevin–Le Châtelier effect to simulate the deformation of notched specimens in tension (smooth and sharp U-notched specimens). This model can be used to account for dynamic strain ageing as suggested by Estrin et al. [Acta Mater. 49 (2000) 1087] but also static strain ageing as suggested by Kubin et al. [Acta Metall. Mater. 40 (1992) 1037]. The experimental material studied is an Al–Cu alloy, displaying dynamic strain ageing at room temperature. Regarding Lüders band propagation, the experimental material studied is a mild steel. This work shows that the PLC serrations disappear progressively on the macroscopic curve when the notch radius decreases. However, strain localization still takes place in the deformed notched zone, and can escape from the notched zone. Regarding the Lüders behavior, the computed spreading of deformation bands is in agreement with experimental observations.

© 2004 Elsevier B.V. All rights reserved.

*Keywords:* Portevin–Le châtelier effect; Lüders behavior; Dynamic strain ageing; Static strain ageing; Finite element simulations

## 1. Introduction

Many engineering materials exhibit strain ageing effects during plastic deformation of flat tensile specimens. Serrations are observed on the macroscopic load/displacement curve, usually attributed to dynamic strain ageing (DSA) and associated with the multisite initiation and propagation of strain rate localization bands [1,2]. Moreover, static strain ageing (SSA) can lead to the propagation of strain localization bands called Lüders bands. One frequent claim for doing this is that, contrary to flat tensile specimens, in real components, the complex geometry including the presence of stress concentrations such as holes and notches generates non-uniform strain fields which tend to absorb and/or dis-

perse strain localization events. The objective of this work is to check that argument both numerically and experimentally.

## 2. Constitutive equations of the macroscopic model of strain ageing

The instabilities simulated in this work occur in some materials, containing interstitial or substitutional elements which may segregate at dislocations and lock them. The constitutive model used in [3] incorporates in a set of phenomenological constitutive equations several features of the intrinsic behavior of strain ageing materials. It tries to mimic, in a phenomenological way, the mechanisms at work in a material volume element: repeated breakaway of dislocations from their solute clouds and recapture, for instance, by mobile solutes. We have cast the evolution equations into the following form in order to comply with the thermodynamics of thermally activated processes. The total deformation

\* Corresponding author. Tel.: +33 1 60 76 30 46;

fax: +33 1 60 76 31 50.

E-mail address: stephanie.graff@ensmp.fr (S. Graff).

is the sum of elastic and plastic strains tensors:

$$\tilde{\varepsilon} = \tilde{\varepsilon}^e + \tilde{\varepsilon}^p, \quad \tilde{\sigma} = \tilde{C} : \tilde{\varepsilon}^e \quad (1)$$

where  $\tilde{C}$  is the fourth-rank tensor of elastic moduli. The criterion is defined by the equation:

$$f(\tilde{\sigma}) = J_2(\tilde{\sigma}) - R \quad (2)$$

The second invariant of the stress tensor is denoted by  $J_2$ . The plastic flow rule is deduced from the normality rule:

$$\tilde{\varepsilon}^p = \dot{p} \frac{\partial f}{\partial \tilde{\sigma}}, \quad \dot{p} = \dot{\varepsilon}_0 \exp\left(-\frac{E_a}{k_B T}\right) \exp[\langle f(\tilde{\sigma}) \rangle V_a / (k_B T)] \quad (3)$$

where  $\dot{p}$  is the viscoplastic multiplier and  $\langle f(\tilde{\sigma}) \rangle$  means the maximum of  $(f(\tilde{\sigma}), 0)$ . In a viscoplasticity theory, the multiplier is given by an independent Eq. (3), where  $T$  is the absolute temperature,  $V_a$  the activation volume, and  $E_a$  the activation energy. Strain hardening is assumed to be isotropic and includes also the strain ageing term ( $P_1 C_s$ ):

$$R = R_0 + Q[1 - \exp(-bp)] + P_1 C_s, \\ C_s = C_m[1 - \exp(-P_2 p^\alpha t_a^n)] \quad (4)$$

where  $R_0$ ,  $Q$ ,  $b$  and  $P_1$ ,  $P_2$ ,  $\alpha$ ,  $n$  are constants,  $C_s$  the concentration of solute atoms segregating around the dislocations which are temporarily immobilized by extrinsic obstacles (“forest dislocations”) and  $C_m$  the saturated concentration around the dislocations. The time dependence of this segregation process can be described the “relaxation–saturation” kinetics of Avrami and can be expressed as suggested in [3] by

$$t_a = \frac{t_w - t_a}{t_w}, \quad t_w = \frac{\omega}{\dot{p}} \quad (5)$$

The ageing time  $t_a$  is the time of the diffusion of the solute atoms towards or along the dislocations. The waiting time  $t_w$  is the mean waiting time of dislocations, which are temporarily stopped by extrinsic obstacles. It depends on the plastic strain rate and can be expressed by Eq. (5).  $\omega$  is the increment of the plastic strain, which is produced when all the stopped dislocations overcome their obstacles.

The previous model has been implemented in the finite element program *Z-set* [4]. The differential equations are integrated at each Gauss point of each element using a Runge–Kutta method of fourth order with automatic time–stepping. The resolution method for equilibrium is based on an implicit Newton algorithm. The elements used in all presented simulations are 8-node quadratic elements with reduced integration (four Gauss points per element) under plane stress conditions.

### 3. Finite element simulations

The parameters used are given in Table 1, for the Al–Cu alloy (hardened duralumin with 4(wt.% Cu)) and the mild

Table 1

Parameters used to simulate the Portevin–Le Chatelier effect in an Al–Cu alloy (after [3]) and the Lüders behavior in a mild steel (after [5])

| Parameters            | Units                                | Al–Cu            | Mild steel           |
|-----------------------|--------------------------------------|------------------|----------------------|
| Young’s modulus       | MPa                                  | 70.2             | 210                  |
| Poisson’s ratio       | –                                    | 0.3              | 0.3                  |
| $R_0$                 | MPa                                  | 140              | 220                  |
| $Q$                   | MPa                                  | 140              | 42                   |
| $b$                   | –                                    | 29               | 20                   |
| $P_1$                 | MPa (at.%) <sup>–1</sup>             | 11               | 30                   |
| $P_2$                 | s <sup>–n</sup>                      | 3.91             | 0.01                 |
| $w$                   | –                                    | 10 <sup>–4</sup> | 2 × 10 <sup>–4</sup> |
| $\alpha$              | –                                    | 0.44             | 0                    |
| $n$                   | –                                    | 0.33             | 1                    |
| $E_a$                 | eV                                   | 0.15             | 1                    |
| $V_a$                 | nm <sup>3</sup> (at.%) <sup>–1</sup> | 11               | 4000                 |
| $C_m$                 | at.%                                 | 2                | 1                    |
| $\dot{\varepsilon}_0$ | s <sup>–1</sup>                      | 10 <sup>–5</sup> | 10 <sup>2</sup>      |
| Initial $t_a$         | s                                    | 0                | 1000                 |

steel alloy (0.15%) at room temperature. The main difference in both sets of parameters is the initial value of  $t_a$ , which is chosen such that initially the concentration of solute atoms  $C_s$  is either minimal or maximal.

Three types of flat tensile specimens are considered: straight specimens, as well as smooth U-notched specimens with a radius equal to 20 mm and sharp U-notched specimens with a radius equal to 1 mm. The ligaments of the notched specimens are identical, equal to 20 mm and their total length of them is equal to 150 mm. The vertical displacement at the bottom is fixed to 0. The vertical displacement of the top is prescribed at a constant displacement rate equal to  $3.33 \times 10^{-2}$  mm s<sup>–1</sup> for the straight specimen and equal to  $7.5 \times 10^{-2}$  mm s<sup>–1</sup> for the U-notched specimens. One node is fixed also with respect to the horizontal direction. In our simulations, plastic strain did not exceed 5% in the deformed part of the specimens.

### 4. Simulations of the PLC effect in notched Al–Cu alloy specimens

Simulations of the PLC effect on straight specimens in 2D and 3D were reported in [3]. We have carried out similar computations to validate our finite element implementation. After a certain amount of plastic strain, slight serrations appear on the macroscopic stress/strain curve. Simultaneously, two strain rate localization bands start to develop on each side of an initial defect (here a slightly lower yield stress in one element). They propagate through the whole specimen and are reflected at the top and bottom boundaries. If fillets are introduced, they generate stress concentrations that are sufficient to trigger similar strain rate localization bands. Each serration on the overall curve is associated with a reflection of the band at one end of the specimen.

Tensile tests were simulated on different U-notched specimens. The results can be divided into two groups. The

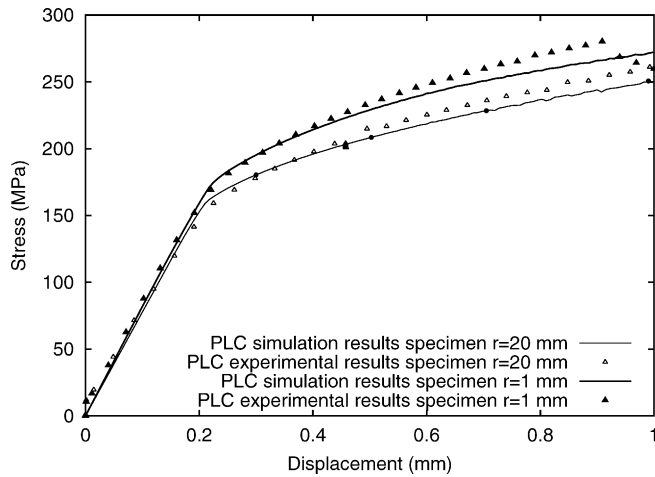


Fig. 1. Normalized overall PLC load divided by the area/displacement curves for the simulated U-notched specimens and the experimental U-notched specimens ( $r = 20$  mm and 1 mm). The points correspond to different overall displacement levels (0.3, 0.5, 0.7, 1 mm), as presented on Fig. 2.

overall load divided by the area/displacement curves are obtained from a smooth U-notched specimen, displaying serrations as in the case of straight tensile specimen (see Fig. 1). Plastic strain rate bands start from the location of stress concentrations at the notches and propagate in the

plastically deformed zone. These different steps are shown in Fig. 2. The contour maps show the variable  $\dot{\rho}$ . Note that some bands are able to escape from the main deformation zone. The scenario is almost similar in the case of sharp U-notched specimens. However, serrations are not observed on the overall load/displacement curve contrary to the smooth U-notched specimen considered above (see Fig. 1). The calculations show that strain rate localization band initiation and propagation over short distances do exist even though serrations are not seen on the overall curve.

### 5. Simulations of the Lüders behavior in notched mild steel specimens

The equations of the model recalled in Section 2 can be used to describe tensile behavior with an initial yield drop, as seen in many mild steels. When applied to the straight flat tensile specimen, such a constitutive response, leads to the formation of a plastic strain localization band starting from an initial defect. The band then propagates over the entire specimen but does not reflect at the specimen ends, contrary to the previous PLC strain rate bands. The specimen then deforms homogeneously, due to the hardening part, as explained in [5,6].

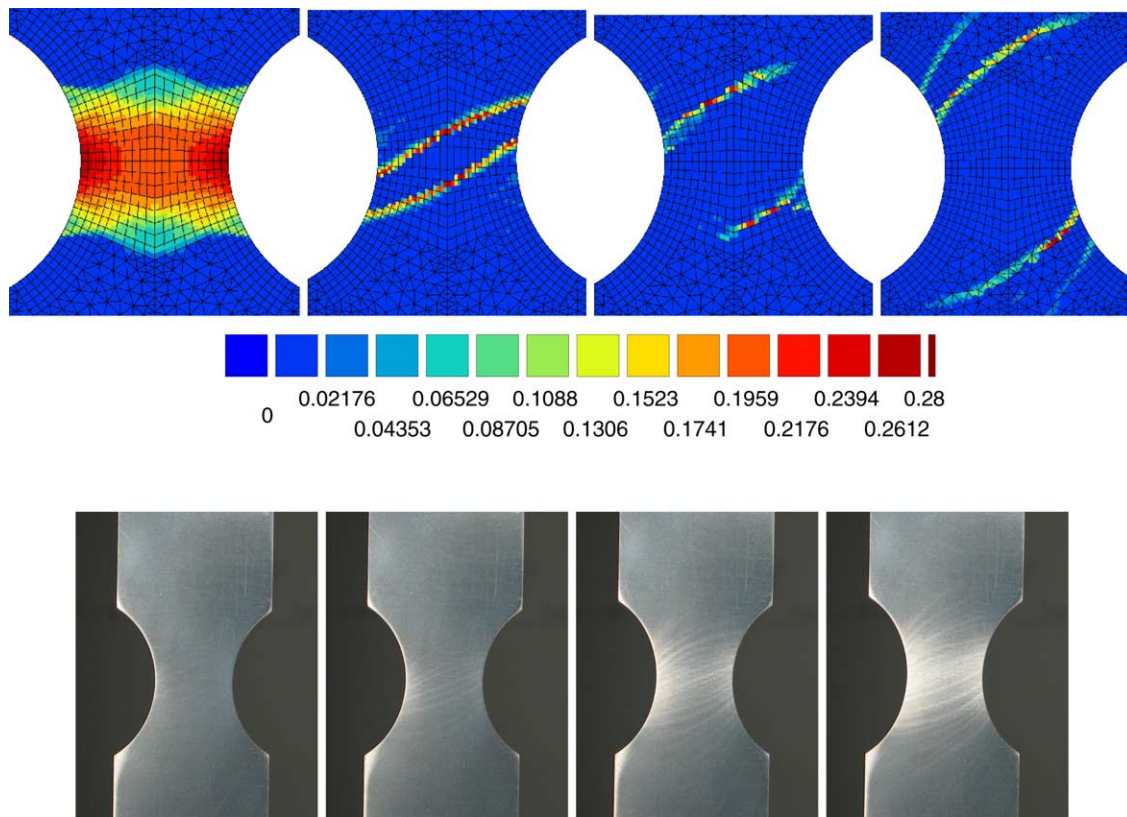


Fig. 2. The PLC effect in a simulated smooth U-notched specimen and an experimental smooth U-notched specimen: plastic strain rate maps at different overall displacement levels (0.3, 0.5, 0.7, 1 mm), which are defined by the points on Fig. 1.

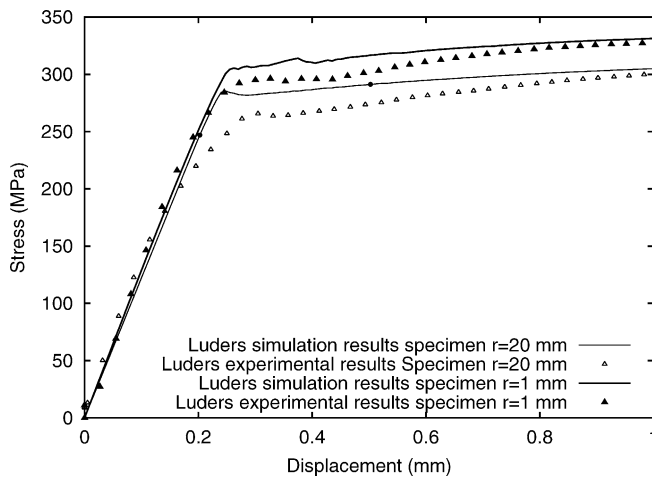


Fig. 3. Normalized overall Lüders load divided by the area/displacement curves for the simulated U-notched specimens and the experimental U-notched specimens ( $r = 20$  mm and 1 mm). The points correspond to different overall displacement levels (0.2, 0.5, 1.2, 1.8 mm), as presented on Fig. 4.

Tensile tests were simulated on different U-notched specimens. The overall load divided by the area/displacement curves display an initial yield drop, which is less pronounced than in straight specimens (see Fig. 3). The initial yield drop decreases with the decrease of the notch radius. The strain bands start from the location of stress concentration at the

notches and they migrate toward the center of the main deformation zone (see Fig. 4).

## 6. Experiment vis-à-vis simulation results

Tensile tests were carried out for the different geometries of flat specimens and for both materials Al–Cu alloy and mild steel at room temperature. The thickness of the specimen was equal to 1 mm. The tests were carried out at the same mean strain rate for the straight specimens and also for the notched specimens. An experimental set-up was developed in order to observe the evolution of polished specimens during the tests. It is composed by a digital camera, a halogen lamp, a tensile machine and a computer.

Considering the PLC effect, the main consequence is that the serrations on the macroscopic experimental and simulated curves disappear when the notch radius decreases. Even though serrations are not observed on the macroscopic experimental curve for the sharp U-notched specimen, the simulations predict strain rate localization bands, which are able to escape from the notched zone (see Figs. 1 and 2). Considering the Lüders behavior, experiments and simulations are in good accordance (see Figs. 3 and 4).

In addition to that, the simulations, which show the localized stress concentrations, are in good accordance with the fracture processes. Indeed, experimentally, the smooth

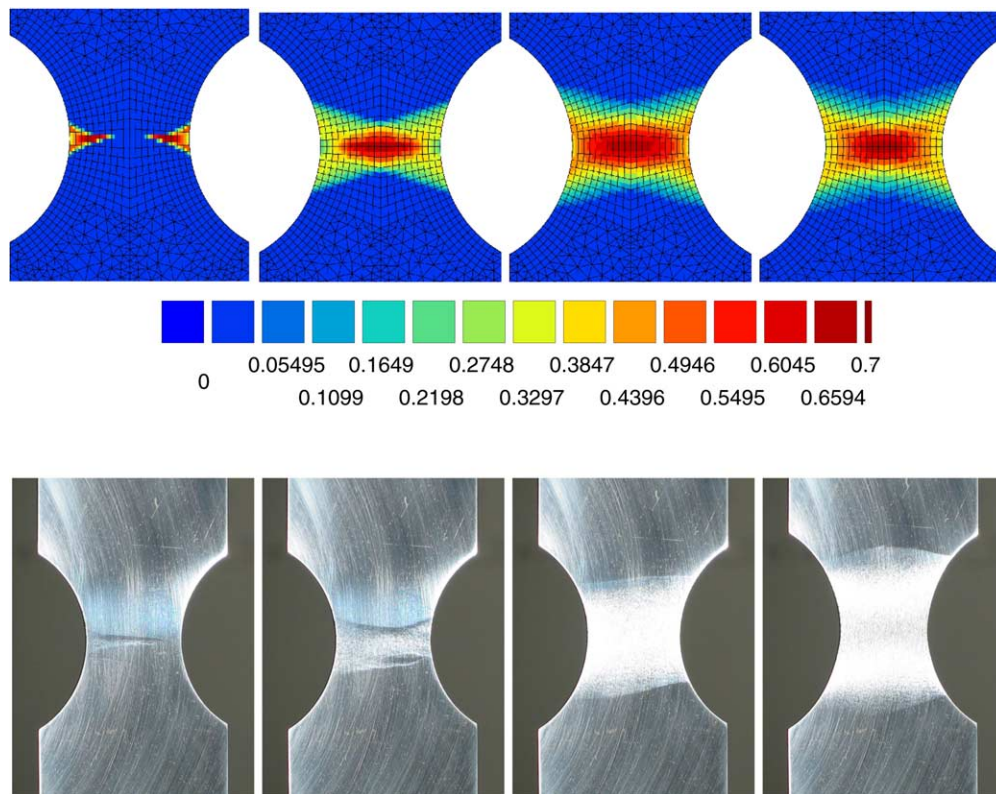


Fig. 4. The Lüders behavior in a simulated smooth U-notched specimen and an experimental smooth U-notched specimen: plastic strain maps at different overall displacement levels (0.2, 0.5, 1.2, 1.8 mm), which are defined by the points on Fig. 3.

U-notched specimens tend to fracture in the middle of the deformed zone for both materials, and the sharp U-notched specimens tend to fracture at the notches for both materials.

## 7. Conclusion

This work shows that the available constitutive model considered simulates the PLC and the Lüders effects for different notched specimens in tension: on the whole, the simulations and the experiments for the Al–Cu alloy and the mild steel are in good accordance. Serrations on the overall load/displacement curves were shown to disappear progressively when the notch radius decreases. Strain rate localization bands initiation and propagation are still predicted by the computation but the spatial propagation range strongly

decreases. The same methodology was used in the case of Lüders band propagation.

These localization phenomena, though not visible on the macroscopic curves, can play a significant role in early fracture processes.

## References

- [1] A. Van den Beukel, *Phys. Stat. Sol.* 30 (1975) 197–206.
- [2] Y. Estrin, L.P. Kubin, *J. Phys.* III 1 (1991) 929–943.
- [3] Y. Estrin, S. Zhang, P.G. McCormick, *Acta Mater.* (2000) 1087–1094.
- [4] Z set package, <http://www.nwnumerics.com>, <http://www.mat.enscm.fr>, 1996.
- [5] S. Forest, *J. Mech. Behav. Mater.* 11 (1997) 45–50.
- [6] T. Lung, H. Tsukahara, *Mater. Sci. Eng. A* 248 (1998) 304–308.